Chitosan hydrogels embedding hyper-crosslinked polymer particles as reusable broad-spectrum adsorbents for dye removal

Martina Salzano de Luna[a,b], Rachele Castaldo[a,c], Rosaria Altobelli[a], Lucia Gioiella[a], Giovanni Filippone[a,*], Gennaro Gentile[c,*], Veronica Ambrogi[a,c]

[a] *Department of Chemical, Materials and Production Engineering (INSTM Consortium – UdR Naples), University of Naples Federico II, P.le Tecchio 80, 80125 Naples, Italy*

[b] *Institute for Polymers, Composites and Biomaterials, National Research Council of Italy, P.le E. Fermi 1, 80055, Portici (NA), Italy*

[c] *Institute for Polymers, Composites and Biomaterials, National Research Council of Italy, Via Campi Flegrei 34, 80078 Pozzuoli, Italy*

Corresponding authors:
*e-mail: gfilippo@unina.it; phone: +39 0817682104 (Giovanni Filippone)
*email: gennaro.gentile@ipcb.cnr.it; phone: +39 0818675057 (Gennaro Gentile)

E-mail addresses of all authors:
Martina Salzano de Luna (martina.salzanodeluna@unina.it); Rachele Castaldo (rachele.castaldo@unina.it); Rosaria Altobelli (rosaria.altobelli@unina.it); Lucia Gioiella (luciagioiella@gmail.com); Giovanni Filippone (gfilippo@unina.it); Gennaro Gentile (gennaro.gentile@ipcb.cnr.it); Veronica Ambrogi (ambrogi@unina.it).

ABSTRACT.

The removal of dye and toxic ionic pollutants from water is an extremely important issue that requires systematic and efficient adsorbent preparation strategies. To address this challenge, we developed composite chitosan (CS)-based hydrogels containing hyper-crosslinked polymer (HCP) particles to be used as broad-spectrum adsorbents. The goal is to efficiently combine the dye adsorption ability of chitosan and the capacity of the porous particles of trapping pollutant molecules. The HCP particles are well distributed and firmly embedded into the chitosan matrix and the composite hydrogels exhibit improved mechanical properties. Adsorption experiments reveal a synergistic effect between CS and HCP particles, and the samples are able to remove both anionic and cationic dyes (indigo carmine, rhodamine 6G and sunset yellow) from water. The maximum dye uptake is higher than that of comparable biosorbents. Moreover, the mechanical properties of the composite hydrogels are enhanced respect to pure CS, and the samples can be regenerated and reused keeping their adsorption ability unaltered over successive cycles of adsorption, desorption, and washing.

1. INTRODUCTION

With the rapid development of economy and the modern industry, water pollution represents a rising environmental concern due to the disposal of large amounts of dye-bearing wastewater from industries. Adsorption of pollutants onto substrates has been recognized as one of the most promising approaches for water purification thanks to its high versatility and relatively low-cost (Forgacs, Cserhati, & Oros, 2004; Yagub, Sen, Afroze, & Ang, 2014). Nowadays, a large variety of non-conventional materials is being explored as potential eco-friendly solutions for wastewater treatment (Crini, 2006). Chitosan (CS) is often regarded as the staple material for the development of green adsorbents due to its excellent biocompatibility, biodegradability and abundance of chelating groups (Bhatnagar & Sillanpää, 2009; Vakili et al., 2014; Olivera et al., 2016). Different kinds of CS-based materials have been recently studied and applied in water treatment, and some of them exhibit outstanding adsorption performances (Ngah, Teong, & Hanafiah, 2011; Dotto, Moura, Cadaval, & Pinto, 2013; Esquerdo, Cadaval, Dotto, & Pinto, 2014). However, the adsorption capacity of this class of materials is not broad-spectrum: the amine and hydroxyl groups of CS indeed act as active sites for trapping mainly anionic pollutants, while the effectiveness towards cationic dyes is rather scarce due to adverse electrostatic interactions (Crini & Badot, 2008). More in general, the concept of broad-spectrum adsorbents has received great attention in recent years. The challenge is the development of adsorbent materials able to simultaneously remove anionic and cationic pollutants from wastewater. Nonetheless, the literature in this field is still rather poor, being often focuses on the employ of nanoparticles with amphiphilic features, such as graphene oxide (GO) (Ramesha, Kumara, Muralidhara, & Sampath, 2011). A notable result was recently obtained by Xiao et al., who demonstrated that L-cysteine reduced graphene oxide exhibits a super-high capacity in
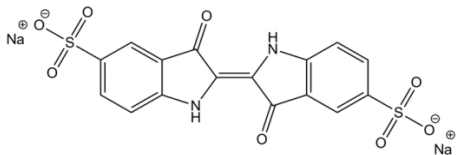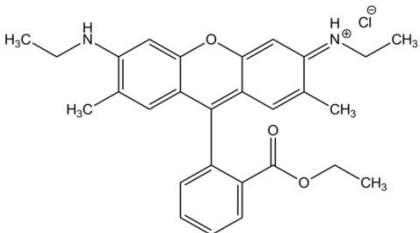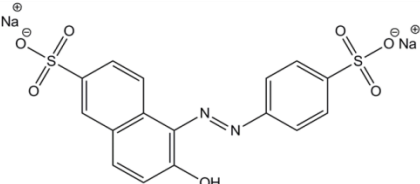
adsorbing both anionic and cationic dyes (Xiao et al., 2016). However, dealing with nanoparticles may raise non-trivial issues in terms of safe use, recovery and possible reuse of the material. From this point of view, the use of monolithic adsorbents is preferable. In this context, one possible strategy consists in binding the nanoparticles through small amounts of a cross-linking polymer. In this way Wang et al. prepared GO-based hydrogels that can adsorb Ponceau S and Trypan blue (Wang et al., 2014). Rather than using the polymer as mere binding agent, one can select a matrix able by itself to carry out adsorbent action, possibly improving the performance of the particles. Following such an approach, Chen et al. developed GO/CS composite hydrogels able to remove both cationic Methylene blue, affine to GO, and anionic Eosin Y, which selectively adsorbs onto CS (Chen, Chen, Bai, & Li, 2013). The main role was played by the nanoparticles, whose adsorbent capacity was preserved by using low amounts of polymer ($\leq$20 wt%) in order to keep most of the functional groups of GO available. Here the emphasis is put on the CS, which represents the dominant component of a composite hydrogel containing relatively low (10 wt%) amounts of hyper-crosslinked polymer (HCP) particles. The idea is exploring the possibility of entrapping pollutant molecules not affine to CS into the inherent micro-and meso-porosity of the HCP particles. Unlike the systems mentioned before, negligible polymer-particle interactions are preferable in our case. The reason is that both the filler porosity and the functional groups of CS have to be preserved. Following this strategy, we have developed a CS/HCP composite hydrogel with high adsorption capacity for both anionic and cationic dyes. We also show that the dye uptake capacity is higher than that of comparable biosorbents. Moreover, the mechanical properties of the composite hydrogels are enhanced respect to pure CS, and the dye removal ability remains unaltered over three successive cycles of adsorption, desorption, and washing.

2. EXPERIMENTAL SECTION

2.1. Materials

Medium molecular weight chitosan (CS) powder (deacetylation degree 75-85%), vinylbenzyl chloride (VBC), p-divinylbenzene (DVB), 2,2′-azobis(2-methylpropionitrile (AIBN), FeCl$_3$, indigo carmine (IC), rhodamine 6G (RH) and sunset yellow (SY) were all purchased from Sigma Aldrich and used without further purification. The classification and molecular structure of the three dyes are shown in Table 1.

Table 1. Classification and molecular structure of the selected dyes.

Commercial name	Dye class	Dye category [a]	Molecular structure
Indigo Carmine (IC)	indigo	anionic	
Rhodamine 6G (RH)	xanthene	cationic	
Sunset Yellow (SY)	single azo	anionic	

[a] According to the classification proposed by Mishra and Tripathy (Mishra Tripathy, 1993).

2.2. Preparation of the HCP particles

HCP particles were prepared by a modified Davankov procedure, consisting in the radical bulk polymerization of the poly(VBC-DVB) precursor followed by hyper-crosslinking of the obtained product by Friedel-Crafts reaction. With respect to conventional suspension or emulsion polymerization approaches (Ahn et al., 2006; Li, Huang, Liang, & Tan, 2010; Fontanals, Marce, Borrull, & Cormack, 2015), the bulk polymerization step allows to significantly reduce the amount of solvent waste, yet ensuring the production of materials with comparable specific surface area (SSA) and adsorption properties (Castaldo et al., 2017). The two-step synthesis is illustrated in Figure 1a.
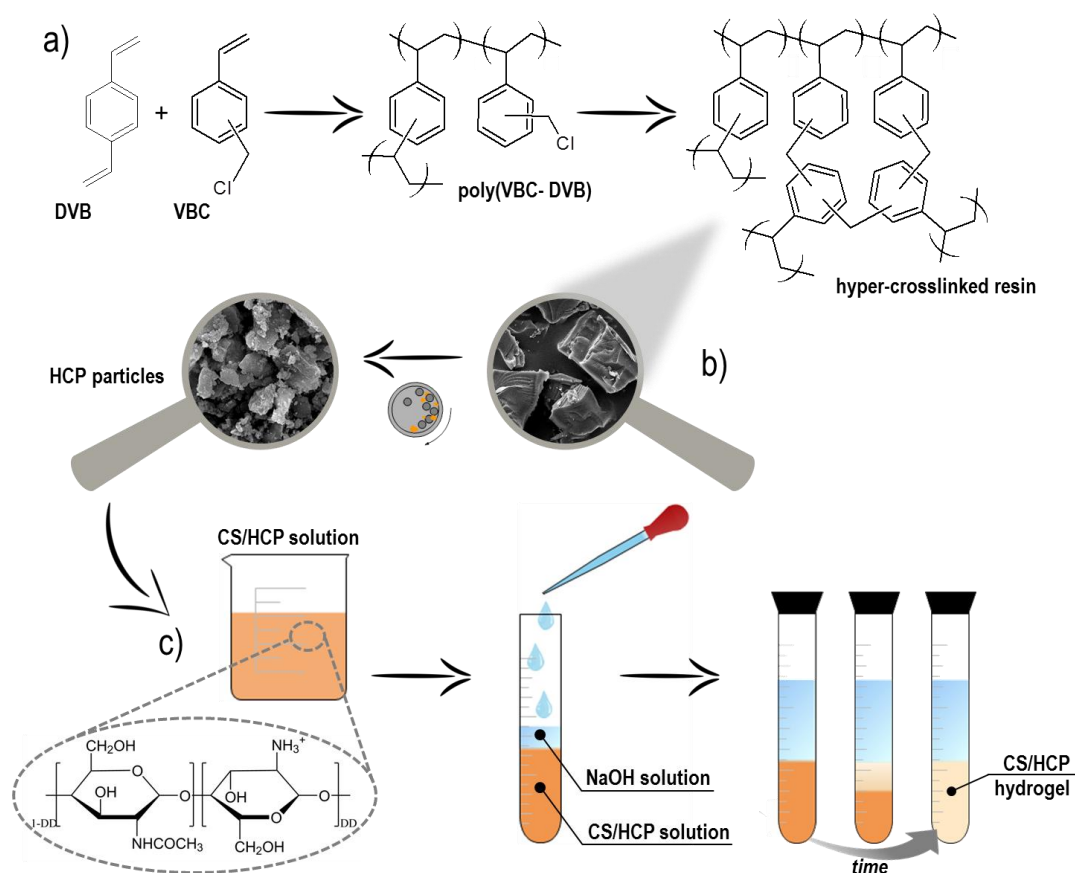

Figure 1. Schematic representation of (a, b) the synthesis of HCP particles and (c) the preparation of the CS/HCP composite hydrogels.

First, VBC and DVB (98/2 mol%) were mixed with 0.5 phr of AIBN under nitrogen flux for 30 min. The mixture was poured in a glass bottle and cured in oven at 80°C for 24 h. The obtained poly(VBC-DVB), which exhibits a slight degree of crosslinking at this stage, was purified by multiple washings with methanol, acetone and diethyl ether, and finally dried under vacuum at 40 °C for 24 h. Afterwards, the poly(VBC-DVB) precursor (2.5 g) was swollen under nitrogen in 1,2-dichloroethane (40 mL) for 2 h. Then the mixtures were cooled down to ~4 °C in an ice/NaCl bath and the Friedel-Crafts catalyst ($FeCl_3$, 2 g) was added (—CH_2Cl:$FeCl_3$ molar ratio of 1:1). The system was heated up to 80 °C, kept at this temperature for 18 h, and finally washed as described for the precursor polymer. During this second step, the chloromethyl groups of VBC create methylene bridges between neighboring phenyl rings, thus introducing new crosslinks. The completion of the hyper-crosslinking reaction was confirmed by Fourier transform infrared spectroscopy (FTIR) and energy dispersive X-ray spectrometry (see Supplementary Material, Section S1). The final product consisted of granules (size in the range 5÷200 μm) composed by an expanded, rigid, three-dimensional polymeric network. The particles were then grinded in a planetary ball-milling system (Retsch PM100) at 600 rpm for 4 hours and using a 125 mL steel milling cup with 10 mm diameter steel spheres (spheres to resin weight ratio of 40:1) (Figure 1.b). This process reduced the size of the HCP particles down to 0.05÷5 μm (see also Supplementary Material, Section S2) while preserving high SSA (1092 ± 19 m^2 g^{-1}).

2.3. Preparation of the CS/HCP composite hydrogels

Chitosan (3 wt/vol%) was dissolved at room temperature in a 98/2 vol/vol% mixture of bi-distilled water and acetic acid via magnetic stirring at room temperature for 72 h. The HCP particles (10 wt% with respect to CS) were added to the CS solution and mixed via magnetic

7

stirring for ~24 h until a homogeneous suspension was obtained. CS and CS/HCP hydrogels were prepared through the phase inversion method (Yao, Li, Yao, & Yin, 2011) (Figure 1.c). In detail, a fixed volume (2 mL) of CS or CS/HCP was poured in glass test tubes, and the same amount of aqueous sodium hydroxide NaOH solution (6 wt/vol%) was carefully poured on the top. The alkaline species diffuse into the CS solution due to the concentration gradient, promoting the formation of a physical hydrogel. The previous conditions for gelation were selected according to a previous study on similar systems (Salzano de Luna et al., 2017). Sedimentation phenomena of the HCP microparticles were found to be negligible in the course of the gelation process. At the end of the process the hydrogels were collected, cut into cylindrical-shaped specimens (diameter 10 mm, thickness ~5 mm), extensively rinsed with bi-distilled water until neutralization, and stored in water until use. The exact amount of HCP particles in the CS/HCP hydrogels was checked through thermogravimetric analysis (Supplementary Material, Section S3).

2.4. Characterization

FTIR analyses were carried out with a Perkin Elmer Spectrum One FTIR spectrometer at a resolution of 4 cm^{-1} and 32 scan collections. The measurements were performed in transmission mode by using disks obtained by compressing the sample powder with potassium bromide. Scanning electron microscopy (SEM) analyses were carried out using a FEI Quanta 200 FEG microscope in high vacuum mode. Energy Dispersive X-ray (EDX) analysis was performed on the precursor and the hyper-crosslinked resins by using an Oxford Inca Energy System 250 and an Inca-X-act LN2-free analytical silicon drift detector. The analyses were performed at 30 kV acceleration voltage. Average results and standard deviation values are based on three

consecutive measurements on different areas of each sample. Before SEM observations, the hydrogels were cryo-fractured and sputter coated with a 15 nm thick Au–Pd layer. All samples were observed at 10 kV acceleration voltage using a secondary electron detector.

Gas adsorption measurements were performed on the HCP particles and the freeze-dried hydrogels using a Micromeritics ASAP 2020 analyzer with high purity gases (>99.999%). Prior to the analysis the samples were degassed under vacuum ($<10^{-5}$ mbar) at 120 °C (HCP particles) or 70 °C (freeze-dried hydrogels). The specific surface area was determined using the Brunauer-Emmett-Teller (BET) equation. Non-local density functional theory (DFT) was applied to the nitrogen adsorption isotherm curves to evaluate the pore size distribution.

The mechanical behavior of the swollen hydrogels was investigated by unconfined compression tests on specimens fully immersed in bi-distilled water. Cylindrical-shaped samples (cross section A_0, height h_0) were placed between the parallel plates of a rheometer (mod. AR-G2 by TA Instruments) and squeezed at compression rate $\dot{h} = 5$ µm s^{-1}. The normal force, F_N, and plate displacement, Δh, were recorded during time. The engineering stress, σ, and strain, ε, were calculated as $\sigma = F_N/A_0$ and $\varepsilon = \Delta h/h_0$. The compressive modulus, E_c, was then estimated in the linear region of the σ-ε curve. Five independent measurements were carried out for each sample.

The swelling ratio, SR, of the hydrogels was calculated from the weight change before and after drying by using the following equation:

$$SR = \frac{W_s - W_d}{W_s}$$
(1)

where W_s and W_d represent the weight of the hydrogel fully swollen in bi-distilled water and dried, respectively.

The dye adsorption behavior of the samples was investigated through equilibrium batch adsorption tests. Mono-component dye solutions at different concentrations (20-1000 mg L^{-1})

9

were prepared from stock solutions and placed in glass flasks. One cylindrical-shaped hydrogel sample (diameter 10 mm, thickness ~5 mm) was added to each flask. In all the experiments, the ratio between adsorbent mass (in mg, dry basis) and volume of dye solution (in mL) was kept equal to one. The flaks were agitated at 150 rpm and T=25 °C using a thermostated agitator (SKI 4, Argo Lab). The adsorption experiments were all performed in neutral pH conditions. The dye concentration was determined using a spectrophotometer at the characteristic maximum absorbance wavelength of each dye (611 nm for IC, 527 nm for RH and 482 nm for SY). Equilibrium was assumed when the dye concentration in the solution proved to be stable over three consecutive measurements. All the experiments were carried out in replicate, and blanks were performed. The equilibrium adsorption capacity, q_e, was determined as:

$$q_e = \frac{V(C_0 - C_e)}{m} \tag{2}$$

where C_0 is the initial dye concentration, C_e is the equilibrium dye concentration, m is the amount of adsorbent, and V is the volume of solution. To test the reusability of the adsorbents, three adsorption-desorption cycles were carried out using the same hydrogel samples. The CS/HCP hydrogels were washed in a 0.1 M NaOH solution (for desorption of IC and SY) or ethanol (for desorption of RH) and then reused. In particular, after the adsorption experiment, each cylindrical-shaped hydrogel was immersed in 10 mL of washing medium and agitated at 150 rpm and T=35 °C using a thermostated agitator for about 24 h. Afterwards, the samples were collected, washed with bi-distilled water, and soaked again in the washing medium. This procedure was repeated three times before performing a new adsorption experiment. The chemical stability of the CS/HCP hydrogels during the regeneration cycles was assessed by TGA (mod. Q500 by TA Instruments). Before the temperature scans, the samples were air-dried

overnight and then subjected to an isothermal treatment at 100°C for 30 minutes to remove the residual water.

3. RESULTS AND DISCUSSION

3.1. Interactions, morphology and mechanical properties

The idea underlying the preparation of the CS/HCP hydrogels is to combine the chemical adsorption ability of the CS and the capacity of the HCP particles to entrap small molecules within their porosity. To fully exploit this working principle, polymer and particles should interact as little as possible in order not to compromise the mutual adsorption capacity. FTIR was employed to study the interactions between the CS and the HCP particles. The FTIR spectra of CS, HCP particles and CS/HCP composite hydrogels are reported in Figure 2.
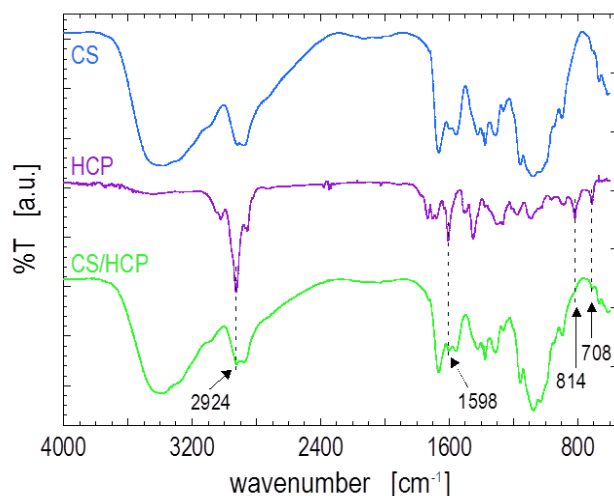

Figure 2. FTIR spectra of CS (blue), HCP (purple) and CS/HCP (green) powders. The spectra have been shifted for the sake of clarity.

11

The spectrum of the HCP particles is characterized by two peaks at 708 cm^{-1} and 814 cm^{-1}, corresponding to aromatic out-plane bending for *p*-substitute benzene, and two bands at 1598 and 2924 cm^{-1}, which are associated to aromatic C=C and aliphatic C–H stretching, respectively (Nagabalasubramanian, Periandy, Mohan, 2010). All these signals can be recognized in the spectrum of the CS/HCP system at the same wavelengths. Similarly, all the characteristic signals of CS remains unaltered in the CS/HCP sample. In particular, for the neat CS sample the carboxamide O=C–NHR and the amine –NH$_2$ bands are located at 1648 cm^{-1} and 1559 cm^{-1} in agreement with the results by Kadir et al. for chitosan films (Kadir, Aspanut, Majid, & Arof, 2011). The same bands appear essentially in the same position in the spectrum of the CS/HCP. The vibrations of –CH$_2$ bending and CH$_3$ symmetrical deformation respectively occur at 1414 cm^{-1} and 1376 cm^{-1} for both CS and CS/HCP samples. The region from 1152 cm^{-1} to 1020 cm^{-1}, which corresponds to the characteristic bands of C–O–C (Ibrahim, Osman, & Mahmoud, 2011), is essentially the same in the neat and composite system. Finally, the C–N fingerprint band appears at 896 cm^{-1} for both CS and CS/HCP samples. In summary, the absence of appreciable variations in the characteristic bands indicates that of negligible chemical interactions establish between the constituents. On the other hand, SEM analyses reveal that the HCP particles are well distributed inside the host CS. The micrographs of the freeze-dried hydrogels and of the HCP particles are shown in Figure 3a-d.
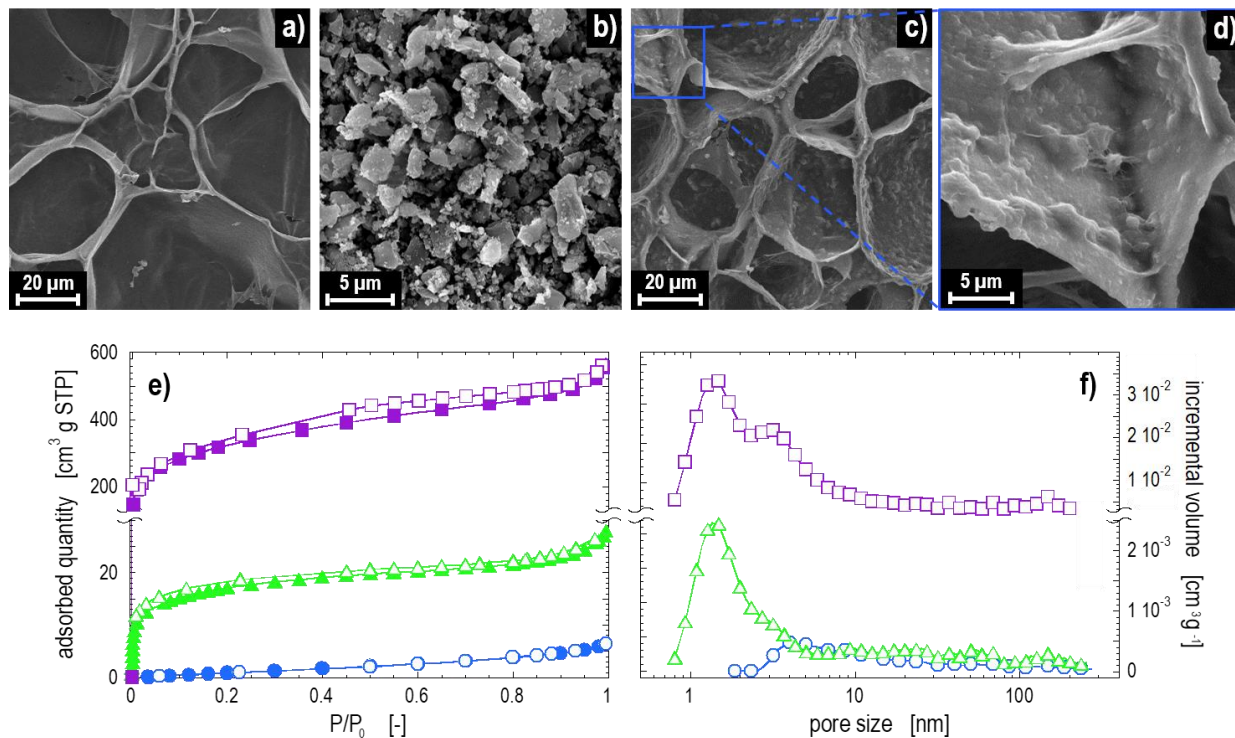
Figure 3. SEM micrographs of (a) CS hydrogel, (b) HCP particles and (c, d) CS/HCP hydrogel. (e) Nitrogen adsorption (full symbols) and desorption (empty symbols) isotherms and (f) DFT pore size distribution of the HCP particles (squares) and the freeze-dried CS (circles) and CS/HCP (triangles) hydrogels.

The removal of water by lyophilization reveals the structure of the CS network, which appears as a labyrinth of pores of few tens of microns. The mesh size is only slightly affected by the HCP particles, whose presence can be inferred from the bumps protruding from the pore walls. A visual inspection of Figure 3c suggests that the HCP particles are evenly distributed in the host CS. It is worth noting that the particles do not lie on the CS walls, being instead embedded in the polymer matrix (Figure 3d). This can be ascribed to the high hydrophobicity of the HCP particles, which accumulate in the CS during gelation rather than in the water phase.

13

Gas adsorption measurements were performed to investigate the porosity of the freeze-dried composite hydrogels. The nitrogen adsorption isotherms and the DFT pore size distribution of HCP particles and freeze-dried hydrogels are reported in Figure 3e and Figure 3f, respectively. The DFT analysis of the HCP particles reveals the presence of two major classes of pores: one with average pore size smaller than 2 nm, and a second family with size distribution centered at about 3 nm. Note that both families of pores are big enough to allow the penetration of the selected dye molecules. The neat CS sample adsorbs extremely low amounts of nitrogen in the adopted conditions. The measurement on the CS/HCP hydrogel reveals that the characteristic porosity of the HCP particles is preserved despite their embedding in the CS matrix. However, the value of specific pore volume was slightly lower than what expected by considering the weight fraction of HCP particles included in the composite. This result can be explained considering that CS partially shrinks during freeze-drying, and part of the pores of the HCP particles can result occluded. Note that the incidence of such occluded porosity on the dye adsorption capacity is probably negligible in the working conditions, viz. in the swollen state. The mechanical behavior is another key aspect of adsorbent materials. Dealing with tough hydrogels allows their easy handling and separation from the liquid phase after use. In addition, mechanically resistant hydrogels can be regenerated without being damaged, and they can be hence eventually reused. Representative stress-strain curves under uniaxial unconfined compression of the swollen CS and CS/HCP hydrogels are shown in Figure 4a. Before testing, the samples were soaked in bi-distilled water until reaching equilibrium configuration. Also note that the water uptake of the chitosan hydrogel was not affected by the presence of HCP particles: the swelling ratio was the essentially same for CS ($SR = 22.6 \pm 0.6$) and CS/HCP ($SR = 22.2 \pm 0.8$) samples.
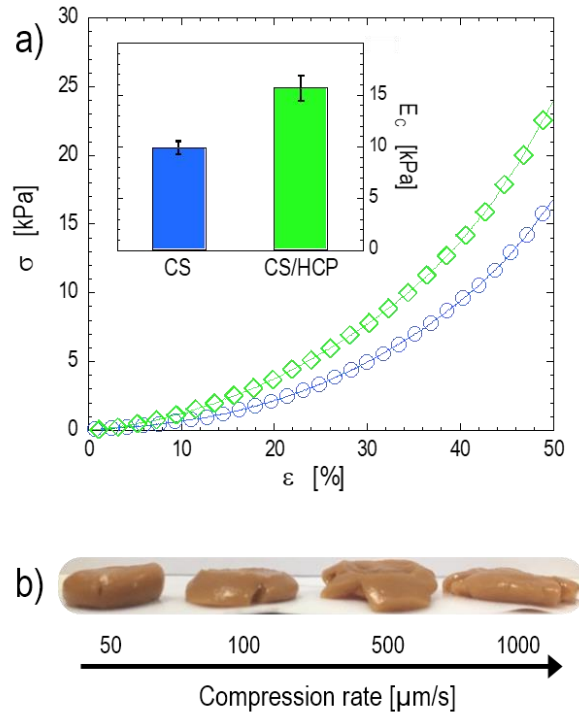
Figure 4. (a) Representative compressive stress-strain curves of the CS (circles) and CS/HCP (diamonds) hydrogels. One point out of ten is shown. The average compressive modulus of the hydrogels is shown in the inset. (b) Images of the CS/HCP hydrogels after mechanical testing at different compression rate.

The two systems share the same overall behavior, characterized by linear σ-ε dependence up to strains of ~15% followed by a strain hardening region. The addition of HCP particles causes an increase of E_c of ~60% (inset of Figure 4a). Such an increase is not coupled with a loss in deformability, which is typically noticed in particulate reinforced composites. In particular, no failure or cracking was observed even when the samples were compressed by half of their initial height ($\varepsilon = 50\%$). Further proofs of the sample toughness emerge from the inspection of samples tested at different compression rates (Figure 4b). When $\dot{h}$ is increased above ~500 µm s^{-1} the

hydrogels lose their initial cylindrical shape, but they keep their integrity without breaking into small pieces. Finally, the water in which the hydrogels were squeezed was collected at the end of the mechanical tests and then filtered to investigate the possible release of HCP particles during sample compression. The same filter used to collect the particles after the ball-milling step were used for this purpose (see Section 2.2). The SEM analysis of the filter surface did not reveal the presence of HCP particles, which suggests that they are firmly embedded within the CS matrix and are not released even in the case of severe sample deformation. Since the leakage of fine particulates would represent an environmental problem (Blackburn, 2004), the latter result is a positive feature of our systems.

3.2. Dye adsorption performances

The adsorption behavior was studied through batch experiments by using Indigo Carmine (IC), Rhodamine 6G (RH) and Sunset Yellow (SY) as model pollutants. The selected dyes differ among them in terms of chemical structure, domain of usage and/or with regard to their chromogen. The equilibrium adsorption capacities of neat CS hydrogels and HCP particles are reported in Figure 5a and 5b as a function of the equilibrium dye concentration.
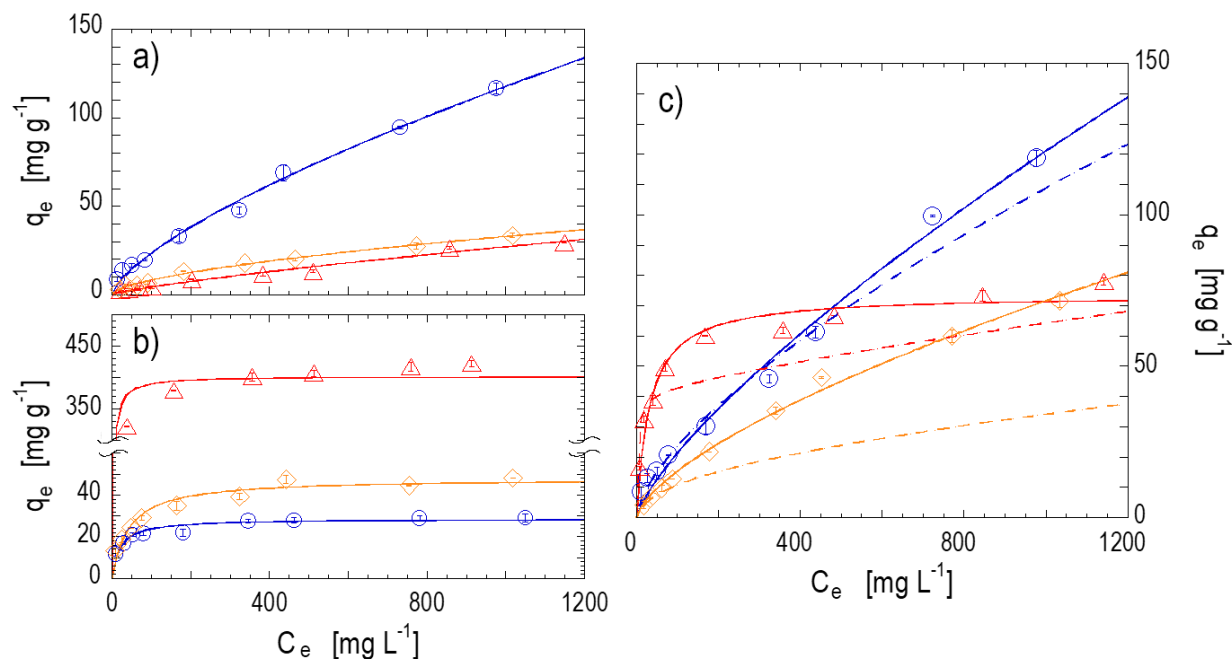
Figure 5. Equilibrium dye adsorption data of IC (blue circles), RH (red triangles) and SY (yellow diamonds) for (a) CS hydrogels, (b) HCP particles and (c) CS/HCP hydrogels. Solid lines in (a-c) are the best fitting of isotherm models (either the Freundlich or the Langmuir model) to the experimental data. The dashed lines in (c) represent the expected behavior of the composite hydrogel calculated according to the mixing rule. Note that error bars (standard deviation over three independent measurements) are smaller than the symbols for each dataset.

The Freundlich model (Freundlich, 1906) is the most suitable to describe the experimental data for the CS hydrogels, whereas the Langmuir model (Langmuir, 1916) better adapts to the adsorption behavior of HCP particles (see Section S4 of the Supplementary Material for details). More importantly, the maximum experimental value of adsorption capacity, q_e^{max}, follows the ranking IC>SY>RH in the case of CS hydrogels, whereas the ranking is RH>SY>IC for the HCP particles. This specular behavior represents the optimal test-bed to investigate the possibility of

17

integrating the adsorption performances of the single constituents in the composite system. The adsorption equilibrium isotherms of the CS/HCP hydrogel are shown in Figure 5c. The overall behavior of the composite is ruled by the component that exhibits higher adsorption capacity for the specific dye. Therefore, the adsorption of IC is dictated by the CS, whereas the HCP particles control the uptake of RH. The best fitting isotherms support this a conclusion: the Freundlich model well fits the equilibrium adsorption data for IC, as in the case of neat CS hydrogel; the Langmuir model is instead better suited to describe the experimental data for RH, which is in line with the results obtained with the HCP particles. On the other hand, the uptake capacities of CS and HCP particles towards SY are comparable, but the Freundlich model better fits the experimental data. This suggests that the CS matrix governs the adsorption of SY in the composite hydrogels. Anyway, the most relevant result that emerges from Figure 5c is the broad-spectrum adsorption capacity of the CS/HCP hydrogels. The high value of q_e^{max} towards IC ensured by the CS is coupled with a good adsorption capacity towards RH and SY, which are mainly ascribed to the HCP particles. It is also important to notice that the adsorption capacities of the composite hydrogels are higher than what expected on the basis of the mixing rule (dashed lines in Figure 5c). In particular, the uptake capacity respect to SY at high C_e is higher than those of both neat constituents. The mechanism behind such a synergic effect is unclear. On the one hand, the HCP particles could somehow locally alter the mesh size of the CS network, thus enhancing the adsorption capacity of the matrix. On the other hand, the CS matrix could block large clusters of dye molecules, which usually form in solution (Giles, MacEwan, Nakhwa, & Smith, 1960) and cannot fit into the pores of the HCP particles.

Due to the more-than-additive action of CS and HCP particles in the composite system, the adsorption performances of the CS/HCP hydrogel are higher than that reported in the literature

for other biosorbents partially or totally made from waste materials. This is shown in Figure 6, where the values of q_e^{max} of the studied systems are compared with selected literature data on systems tested in conditions comparable to those adopted in this study (details are given in Section S5 of the Supplementary Material).
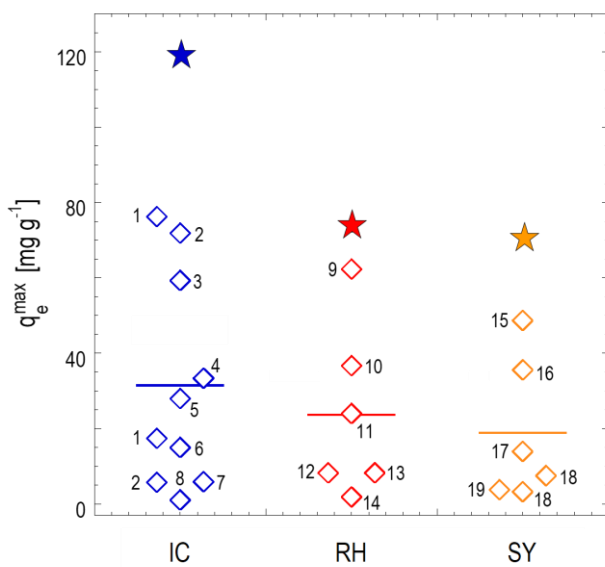

Figure 6. Comparison of the maximum dye adsorption capacity of the CS/HCP hydrogels (full stars) with literature data on biosorbents totally or partially obtained from wastes (empty diamonds). Horizontal solid lines represent the average of the reported literature data. Numbers near symbols indicate the system from literature whose details are given in the Supplementary Material.

The q_e^{max} of the CS/HCP hydrogel is more than three times higher than the average of the literature values for each of the considered dyes (horizontal solid lines in Figure 6). It is worth noting that the maximum adsorption capacity of our system approaches (often exceeding) that of other classes of adsorbents, such as functionalized nanoparticles, metal organic frameworks, or microporous materials, which are usually characterized by high adsorption capacity due to high

19

surface-to-volume ratio and porosity. To give just a few examples: the uptake capacity for IC of the CS/HCP adsorbent (118 mg g^{-1}) is comparable to that of cetyltrimethylammonium bromide-modified TiO$_2$ nanoparticles (106 mg g^{-1}) (Zolgharnein, Bagtash, Asanjarani, 2014); the q_e^{max} towards RH of the composite hydrogel (78 mg g^{-1}) definitely exceeds that of graphene oxide (24 mg g^{-1}) (Ren et al., 2014); in the case of SY, the adsorption ability of the CS/HCP system (72 mg g^{-1}) is twice that of silver nanoparticles loaded on activated carbon (37 mg g^{-1}) and almost equal to that of activated carbon modified with cadmium hydroxide nanowires (77 mg g^{-1}) (Ghaedi, 2012).

The life time and reusability of the CS/HCP hydrogels was also investigated by means of reiterated adsorption-desorption cycles on the same sample. The results indicate that the materials preserve the same dye adsorption capacity even after three cycles of reuse (Figure 7a). The maximum variation of q_e between the first and third adsorption cycle was found to be of less than 5%, suggesting that the CS/HCP systems have a long-lasting efficacy. This aspect is particularly important in practical applications because of stringent ecological and economic demands for sustainability (Sun, Cao, & Lu, 2011; Haldorai & Shim, 2014). Finally, thermogravimetric analyses were carried out to investigate the chemical stability of the CS/HCP hydrogels upon regeneration. The TGA curves of the samples before and after three successive adsorption-desorption cycles are almost superimposed (Figure 7b). Since the CS exhibits molecular weight dependent degradation behavior (Mao et al. 2004), the latter result suggests that negligible degradation phenomena occur during the adsorbent regeneration process.
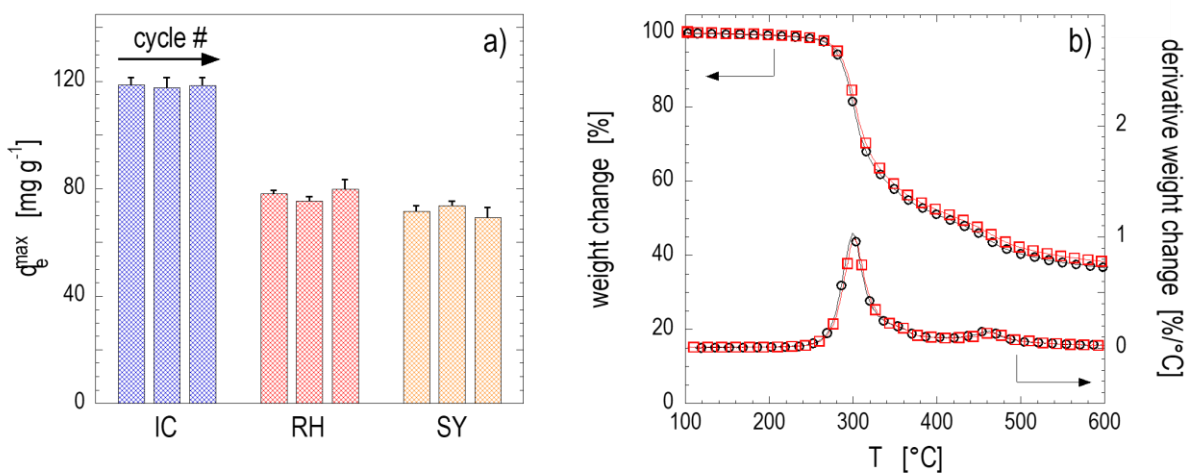
Figure 7. (a) Equilibrium dye adsorption capacity of the CS/HCP hydrogels for three cycle of use. (b) Thermogravimetric curves of CS/HCP hydrogels before (squares) and after (circles) three successive adsorption-desorption cycles: temperature dependent weight change and derivative weight change.

4. CONCLUSIONS

Composite hydrogels were prepared by phase inversion method starting from a chitosan solution filled with hyper-crosslinked polymer particles synthesized by a modified Davankov procedure. The goal was the realization of broad-spectrum adsorbents, which are able to effectively remove both anionic and cationic dyes from water. For this purpose, the constituents of the composite system were selected so as to possess negligible polymer-particle interactions, in order to preserve the porosity of the HCP particles and the ability of chitosan functional groups in trapping anionic pollutant molecules. Despite the poor affinity, the HCP particles resulted well distributed and firmly embedded into the chitosan matrix. This reflected in an improvement in the mechanical properties of the composite CS/HCP hydrogel with respect to the unfilled CS. A

synergistic effect between CS and HCP particles was obtained for the adsorption properties of the composite CS/HCP hydrogels, which exhibited excellent uptake capacity for all the investigated dyes. Finally, the dye removal ability remains unaltered over three successive adsorption-desorption cycles.

APPENDIX A. SUPPLEMENTARY DATA

Supplementary data associated with this article can be found in the online version.

NOTES

REFERENCES

Ahn, J. H., Jang, J. E., Oh, C. G., Ihm, S. K., Cortez, J., & Sherrington, D. C. (2006). Rapid generation and control of microporosity, bimodal pore size distribution, and surface area in Davankov-type hyper-cross-linked resins. *Macromolecules*, *39*, 627-632.

Bhatnagar, A., & Sillanpää, M. (2009). Applications of chitin-and chitosan-derivatives for the detoxification of water and wastewater—a short review. *Advances in Colloid and Interface Science*, *152*, 26-38.

Blackburn, R. S. (2004). Natural polysaccharides and their interactions with dye molecules: applications in effluent treatment. *Environmental Science & Technology*, *38*, 4905-4909.

Castaldo, R., Avolio, R., Cocca, M., Gentile, G., Errico, M. E., Avella, M., Carfagna, C., & Ambrogi, V. (2017). A versatile synthetic approach towards hyper-crosslinked styrene-based polymers and nanocomposites. *Macromolecules*, *50*, 4132-4143.

Chen, Y., Chen, L., Bai, H., & Li, L. (2013). Graphene oxide–chitosan composite hydrogels as broad-spectrum adsorbents for water purification. *Journal of Materials Chemistry A*, *1*, 1992-2001.

Crini, G. (2006). Non-conventional low-cost adsorbents for dye removal: a review. *Bioresource Technology*, *97*, 1061-1085.

Crini, G., & Badot, P. M. (2008). Application of chitosan, a natural aminopolysaccharide, for dye removal from aqueous solutions by adsorption processes using batch studies: a review of recent literature. *Progress in Polymer Science*, *33*, 399-447.

Dotto, G. L., Moura, J. M. D., Cadaval, T. R. S., & Pinto, L. A. D. A. (2013). Application of chitosan films for the removal of food dyes from aqueous solutions by adsorption. *Chemical Engineering Journal*, *214*, 8-16.

Esquerdo, V. M., Cadaval, T. R. S., Dotto, G. L., & Pinto, L. A. A. (2014). Chitosan scaffold as an alternative adsorbent for the removal of hazardous food dyes from aqueous solutions. *Journal of Colloid and Interface Science*, *424*, 7-15.

Fontanals, N., Marce, R. M., Borrull, F., & Cormack, P. A. G. (2015). Hypercrosslinked

    materials: preparation, characterisation and applications. *Polymer Chemistry*, *6*, 7231-7244.

Forgacs, E., Cserhati, T., & Oros, G. (2004). Removal of synthetic dyes from wastewaters: a

    review. *Environment International*, *30*, 953-971.

Freundlich, H. M. F. (1906). Over the adsorption in solution. *Journal of Physical Chemistry*, *57*,

    1100-1107.

Ghaedi, M. (2012). Comparison of cadmium hydroxide nanowires and silver nanoparticles

    loaded on activated carbon as new adsorbents for efficient removal of Sunset yellow: Kinetics

    and equilibrium study. *Spectrochimica Acta Part A: Molecular and Biomolecular*

    Spectroscopy, *94*, 346-351.

Giles, C. H., MacEwan, T. H., Nakhwa, S. N., & Smith, D. (1960). Studies in adsorption. Part

    XI. A system of classification of solution adsorption isotherms, and its use in diagnosis of

    adsorption mechanisms and in measurement of specific surface areas of solids. *Journal of the*

    Chemical Society, 3973-3993.

Haldorai, Y., & Shim, J. J. (2014). An efficient removal of methyl orange dye from aqueous

    solution by adsorption onto chitosan/MgO composite: A novel reusable adsorbent. *Applied*

    Surface Science, *292*, 447-453.

Ibrahim, M., Osman, O., & Mahmoud, A. A. (2011). Spectroscopic analyses of cellulose and

    chitosan: FTIR and modeling approach. *Journal of Computational and Theoretical*

    Nanoscience, *8*, 117-123.

Kadir, M. F. Z., Aspanut, Z., Majid, S. R., & Arof, A. K. (2011). FTIR studies of plasticized poly (vinyl alcohol)–chitosan blend doped with NH 4 NO 3 polymer electrolyte membrane. *Spectrochimica Acta Part A: Molecular and Biomolecular Spectroscopy*, *78*, 1068-1074.

Langmuir I. (1916). The constitution and fundamental properties of solids and liquids. *JACS*, *38*, 2221–2295.

Li, B., Huang, X., Liang, L., & Tan, B. (2010). Synthesis of uniform microporous polymer nanoparticles and their applications for hydrogen storage. *Journal of Materials Chemistry*, *20*, 7444-7450.

Mao, S., Shuai, X., Unger, F., Simon, M., Bi, D., & Kissel, T. (2004). The depolymerization of chitosan: effects on physicochemical and biological properties. *International Journal of Pharmaceutics*, *281*, 45-54.

Mishra, G., & Tripathy, M. (1993). A critical review of the treatment for decolorization of textile effluent. *Colourage*, *40*, 35-38.

Nagabalasubramanian, P. B., Periandy, S., & Mohan, S. (2010). Ab initio HF and DFT simulations, FT-IR and FT-Raman vibrational analysis of α-chlorotoluene. *Spectrochimica Acta Part A: Molecular and Biomolecular Spectroscopy*, *77*, 150-159.

Ngah, W. W., Teong, L. C., & Hanafiah, M. A. K. M. (2011). Adsorption of dyes and heavy metal ions by chitosan composites: A review. *Carbohydrate Polymers*, *83*, 1446-1456.

Olivera, S., Muralidhara, H. B., Venkatesh, K., Guna, V. K., Gopalakrishna, K., & Kumar, Y. (2016). Potential applications of cellulose and chitosan nanoparticles/composites in wastewater treatment: A review. *Carbohydrate Polymers*, *153*, 600-618.

Ramesha, G. K., Kumara, A. V., Muralidhara, H. B., & Sampath, S. (2011). Graphene and graphene oxide as effective adsorbents toward anionic and cationic dyes. *Journal of Colloid and Interface Science*, *361*, 270-277.

Ren, H., Kulkarni, D. D., Kodiyath, R., Xu, W., Choi, I., & Tsukruk, V. V. (2014). Competitive adsorption of dopamine and rhodamine 6G on the surface of graphene oxide. *ACS Applied Materials & Interfaces*, *6*, 2459-2470.

Salzano de Luna, M., Altobelli, R., Gioiella, L., Castaldo, R., Scherillo, & G., Filippone, G. Role of Polymer Network and Gelation Kinetics on the Mechanical Properties and Adsorption Capacity of Chitosan Hydrogels for Dye Removal. *Journal of Polymer Science B: Polymer Physics*, doi: 10.1002/polb.20170188

Sun, H., Cao, L., & Lu, L. (2011). Magnetite/reduced graphene oxide nanocomposites: one step solvothermal synthesis and use as a novel platform for removal of dye pollutants. *Nano Research*, *4*, 550-562.

Vakili, M., Rafatullah, M., Salamatinia, B., Abdullah, A. Z., Ibrahim, M. H., Tan, K. B., Gholami, Z., & Amouzgar, P. (2014). Application of chitosan and its derivatives as adsorbents for dye removal from water and wastewater: A review. *Carbohydrate Polymers*, *113*, 115-130.

Wang, X., Liu, Z., Ye, X., Hu, K., Zhong, H., Yu, J., Jin, M., & Guo, Z. (2014). A facile one-step approach to functionalized graphene oxide-based hydrogels used as effective adsorbents toward anionic dyes. *Applied Surface Science*, *308*, 82-90.

Xiao, J., Lv, W., Xie, Z., Tan, Y., Song, Y., & Zheng, Q. (2016). Environmentally friendly reduced graphene oxide as a broad-spectrum adsorbent for anionic and cationic dyes via π–π interactions. *Journal of Materials Chemistry A*, *4*, 12126-12135.

Yagub, M. T., Sen, T. K., Afroze, S., & Ang, H. M. (2014). Dye and its removal from aqueous solution by adsorption: a review. *Advances in Colloid and Interface Science*, *209*, 172-184.

Yao, K., Li, J., Yao, F., & Yin, Y. (2011). Chitosan-based hydrogels: functions and applications. CRC Press.

Zolgharnein, J., Bagtash, M., & Asanjarani, N. (2014). Hybrid central composite design approach for simultaneous optimization of removal of alizarin red S and indigo carmine dyes using cetyltrimethylammonium bromide-modified TiO2 nanoparticles. *Journal of Environmental Chemical Engineering*, *2*, 988-1000.